Scientific Journal for Damietta Faculty of Science **15**(1) 2025, 82-89
Doi: 10.21608/sjdfs.2025.422525
ISSN Print 2314-8594
ISSN Online 2314-8616

*https://sjdfs.journals.ekb.eg/*

# Landsat-based lithological mapping of the Neoproterozoic rocks in the Egyptian Nubian Shield: Case Study from Wadi Zeidun Area, Central Tectonic Province

Mahmoud N. El-Tawapty[*1], Hoda Ragab Saad[1], Zakaria Hamimi[2], Hosam Khamis[3] and Magdi Khalil[1]

[1]Geology Department, Faculty of Science, Damietta University, New Damietta, Egypt.
[2]Geology Department, Faculty of Science, Benha University, Benha, Egypt.
[3]Nuclear Material Authority, Cairo, Egypt.

Received: 10 February 2025 /Accepted: 24 March 2025

[*]Corresponding author's E-mail: m.eltawapty@du.edu.eg

**Abstract**

Wadi Zeidun area is located south of the Qift-Quseir road, along the western boundary of the Central Eastern Desert (CED). It is covered by a variety of Neoproterozoic rock units, including metaultramafics (both massive and sheared), metagabbros, metavolcanics, volcanoclastic metasediments, arc assemblage, gneissose granite, as well as older and younger granites. These units are unconformably overlain by a post-amalgamation sequence of molasse sediments (Hammamat Group). Post-Hammamat felsites do exist. This study investigates the effectiveness of remote sensing techniques, particularly using Landsat-8 data , fieldwork data and existing geological maps, to map the Neoproterozoic rocks outcropping to the East Wadi Zeidun area. The Landsat-8 data enabled the identification of Hammamat Molasse Sediment, post-Hammamat felsites and granites through the decorrelation stretch of the False Color Composite (FCC) 7:6:5 in RGB. The Principal Component Analysis (PCA) in RGB (PC4, PC3, PC2) successfully distinguished the post-Hammamat felsites, arc assemblage, younger granite and Hammamat Sediments. Furthermore, specific band ratio combinations (BRC) such as (7/5, 5/4, 6/7) and (4/2, 6/5, 6/7) in RGB distinguished ophiolites, metavolcanics, metasediments, Hammamat Sediments, younger granites, and post-Hammamat felsites. The results obtained from image processing were validated through field verification and ground truthing..

***Keywords***: Landsat, Neoproterozoic rocks, Egyptian Nubian Shield, Wadi Zeidun Area, Central Tectonic Province

## Introduction

The area under consideration lies between longitudes of 33˚40′ to 34˚10′ and latitudes of 25˚35′ to 25˚ 57′. It is found to the south of the asphaltic road of the Qift–Quseir road on the western boundary of the CED and is covered with Precambrian basement rocks (Fig.

1). Identifying lithological units and producing geological maps have been achieved through the utilization of various spaceborne multispectral data from sources like Landsat 8 (LS8), as well as hyperspectral remote sensing data (RSD) from instruments such as Hyperion and AVIRIS (e.g. Abrams et al., 1988; Ciampalini et al., 2013; Loughlin, 1991). The digital form of RSD enables image processing methods to retrieve and enhance information relevant to mapping activities. Standard techniques used in remote sensing for identifying and mapping minerals and rocks include band ratio analysis and Principal Component Analysis (PCA) (e.g. Hamimi et al., 2022). The region of the electromagnetic spectrum ranging from visible light to infrared (0.4–14 μm) is generally used to distinguish different minerals and rocks by analyzing their spectral reflectance properties (Hunt, 1977). The spectral differentiation of silicate minerals is achieved through the thermal infrared wavelength range (3–20 μm) which provides additional insights that enhance the information obtained from the visible and near-infrared (VNIR) as well as the shortwave infrared (SWIR) ranges (e.g. Clark, 1999; Gaffey et al., 1993; Hook et al., 1999; Hunt, 1977).

Wadi Zeidun area has previously been explored in several studies (e.g. Abd El-Wahed, 2007; Dixon, 1979; El-Shazly & Khalil, 2016; El-Shazly et al., 2019; Fowler & Hamimi, 2021; Fowler et al., 2007; Fowler et al., 2020; Kassem et al., 2023; Makroum et al., 2001; Sims & James, 1984) (Figs. 2&3). This research aims to locate and delineate different lithological units and geological features within the specified region by using Landsat-8 Operational Land Imager (LS8OLI) data alongside field surveys. A variety of spectral processing approaches, such as PCA and BRC methods, have been chosen to identify the established lithological units within the investigated area.

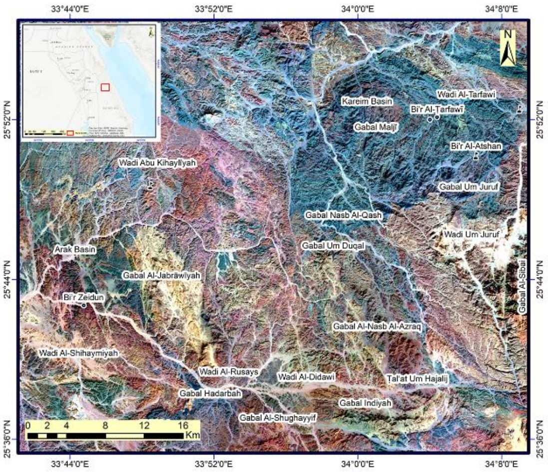


Fig. 1. Wadi Zeidun area location map (RGB-742)

## Geologic Setting

The Neoproterozoic rocks exposing in the study area include ophiolitic metaultramafics, metagabbros, metavolcanics and volcanoclastic metasediments, together with arc assemblage, gneissose granite, and older granites, along with the volcanosedemenatry Hammamat Molasse Sediments. Younger granites, trachyte plugs and sheets, Volcanic rocks cover and not intrude, and post-Hammamat felsites intrude these rocks. The ophiolitic formations are characterized by a lengthy NW-SE belt that showcases moderate to significant relief. They are represented as a collection of extensive, interlinked ultrabasic rock formations (such as talc carbonates) and metagabbros, separated by a thrust contact between them.

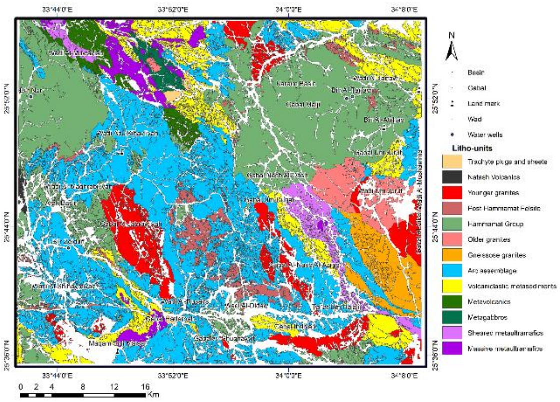


Fig. 2. The geologic map of Wadi Zeidun area (Hamimi et al., 2024)

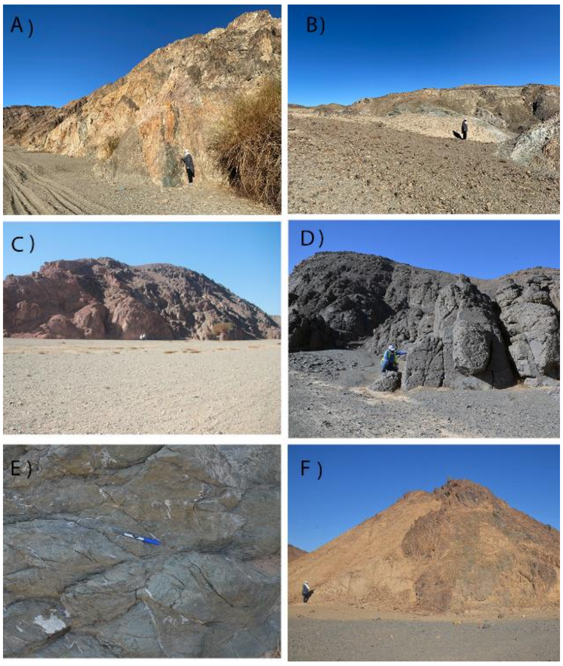


Fig. 3. Field photographs of the litho-units outcropping in the investigated area. A) Gneissose granite intersected by deformed acidic and basic dykes, B) Talc schist located within ophiolitic mélange, C) The contact zone between the alkali granite and the metavolcanics, D) The Hammamat Conglomerates, E) The characteristic shape of pillow lava, and F) The granite prominently displaying a felsic dyke within Wadi Zeidun area.

Felsite dykes penetrate the underlying rocks and molasse sediments, noted for their steeply dipping orientation and primary trends that run north-south (N–S) and northeast-southwest (NE–SW). In the study area, these dykes are frequently located alongside the felsite sills in the northern Zeidun basin and Wadi El-Qash. An alteration zone arises within the molasse sediments due to the intrusion of felsite.

The younger granite is found as oval intrusions in specific locations such as Gabal Um Duqal, Gabal Al-Jabrawiyah,and Gabal Al-Sibai, where it has penetrated the arc assemblage and trends in a NW-SE direction.

## Materials and Methods

The LS8OLI data from the study area underwent thorough radiometric and geometric corrections, which were implemented using ground control points along with a digital elevation model (Lee et al., 2004). LS8 imagery processing was performed with the Environment for Visualizing Images (ENVI 5.3.1) software. The Quick Atmospheric Correction method was applied to convert the digital number values from the LS8 data into reflectance data, effectively minimizing the effects of atmospheric scattering. This method is based on empirically derived average reflectance values obtained from a range of material spectra that are primarily independent of the specific scene (FLAASH Module, 2009).

Images that showcase the red-green-blue (RGB) color blend from LS8OLI existed selected mainly established on the spectral reflectance properties of the predominant rock classes in the Wadi Zeidun region. The color composite technique was utilized to illustrate the multispectral bands of the LS8 data through the use of additive colors—red, green, and blue—where the spectral response of minerals indicates peak reflectance. Bands from both the visible and infrared portions of the electromagnetic spectrum were combined to generate the RGB imagery (Crosta, 1989; Evans, 1988; Gaffey, 1986).

The PCA method was applied to remote sensing data to generate independent output bands, remove noise components, and reduce the complexity of the data's dimensions (e.g., Ciampalini et al., 2013; Hamimi et al., 2022; Loughlin, 1991). The PCA involves identifying a new pack of orthogonal axes that are centered on the data's significance, aimed at maximizing the variance of the data.

Differences in topography, overall changes in reflectance, and variations in brightness associated with grain size can be effectively addressed using the BRC method (e.g. Abdelsalam et al., 2000a; Abdelsalam et al., 2000b; Abrams and Kahle, 1984; Abrams et al., 1983; Hamimi et al., 2022; Sultan et al., 1987). However, this technique tends to accentuate differences in the shape of spectral reflectance. BRC images are produced by splitting the digital numbers (DN) of pixels in a band exhibiting high total reflectance by those of the interconnected pixels in a band showing low total reflectance (Jensen, 1996). The selection of BRC is based on the spectral signatures of the key lithological divisions expected to be present in the area (e.g. Ghrefat et al., 2021; Hamimi et al., 2022).

## Results and discussion

Over 172 rock samples were gathered

utilizing handheld GPS, representing different lithologic units across various stations, with GPS coordinates for each sample site recorded. The locations of the collected samples were transformed into a GIS layer, along with all relevant attribute data. An initial identification of the gathered samples was conducted, in addition to the field observations of noted structures and features at each station. The samples were investigated using a polarizing microscope to identify their key mineral components, textural relationships, and, consequently, the precise lithologic classifications.

The FCC image technique utilizes simple procedures that are commonly used for data presentation. To represent a colored image in a band combination (BC) setting, only three channels (Red, Green, and Blue) are required. For the best selection of the three BC, it is essential to minimize the correlation of the variance values. The FCC technique is well-known for its ability to differentiate rock units based on the spectral signatures of the various minerals found in different rocks. This approach has been applied in the analysis of the research area. Additionally, field data has been instrumental in identifying the different rock types present in the study region.

RGB color composite image derived from the 7–6–5 bands of Landsat-8 data, which is employed for lithological mapping in the area under consideration, reveals distinct color variations that correspond to the different rocks (Fig. 4). The Hammamat Sediments are represented in blue, the post-Hammamat felsites in green, the granite in reddish-blue hue, and the older granite in pinkish-gray tone. The examination of this image holds considerable importance in the creation of the geological map for the corresponding area (Fig. 2).

The PCA method is utilized to generate uncorrelated data with enhanced contrast. In this study, the PCA technique was applied to LS8OLI data using bands 4, 3, and 2 PCA in RGB format to differentiate rock units lithologically (Fig. 5). Most lithological units were recognized and mapped using the PCA FCC image. This analysis specifically emphasizes the post-Hammamat Felsites in green, the arc assemblages in dark orange-pink hues, the younger granite in bright orange-pink and yellow, and the Hammamat Sediments in blue (Fig. 5).

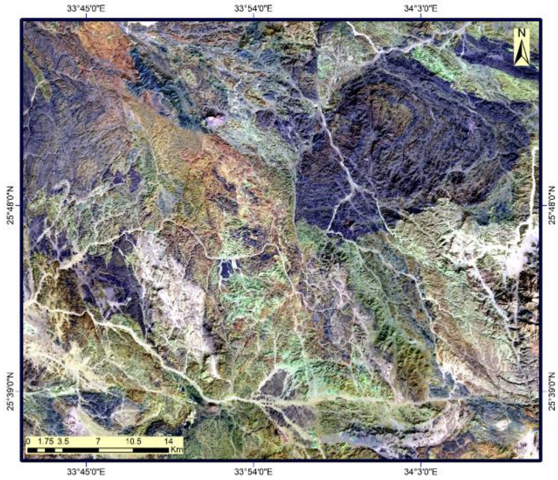


Fig. 4 False-color composite (FCC) that utilizes bands 765 in RGB from the LS8OLI dataset of the Wadi Zeidun area. The Hammamat Sediments are depicted in blue, the post-Hammamat Felsites are shown in green, the granite appears as a reddish blue, and the older granite is illustrated in a pinkish gray shade.

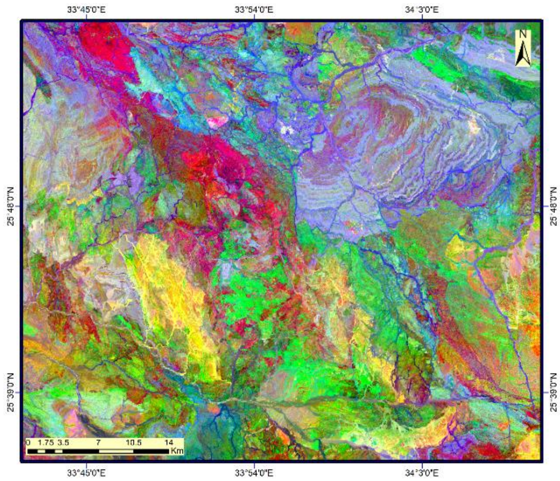


Fig. 5 Principal Component Analysis of Wadi Zeidun area using PCA RGB (PC4, PC3, PC2) based on Landsat-8 data. It highlights the post-Hammamat Felsites in green, the arc assemblage in dark orange and pink hues, the younger granite in bright orange, pink, and yellow shades, and the Hammamat Sediments in blue.

The classification of lithological units was conducted using the BRC technique applied to the Landsat data (e.g. FREI and Jutz, 1990; Abdelsalam and Stern, 1999; Sabins, 1999; Kusky and Ramadan, 2002; Ghrefat et al., 2021; Hamimi et al., 2022).

The BRC (7/5, 5/4, 6/7) presented in RGB for the concerned area highlighted the ophiolites in bright blue, while the metavolcanics and the metasediments are depicted in reddish-yellow and orange (Fig. 6). The Hammamat Sediments appear in green and bluish green (turquoise); the younger granites are shown in greenish-yellow, and the post-Hammamat Felsites are represented in pale blue.

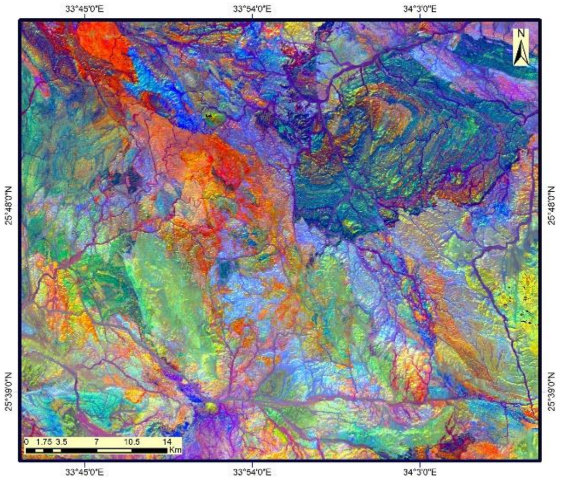


Fig. 6. The RGB band ratio (7/5, 5/4, 6/7) of Wadi Zeidun area highlights ophiolites in bright blue, with metavolcanics and metasediments represented in reddish-yellow and orange hues. The Hammamat Sediments are displayed in green and bluish green (turquoise), while the younger granites appear in greenish-yellow shade, and the post-Hammamat Felsite are illustrated in a soft pale blue.

The band ratio (4/2, 6/5, 6/7) illustrated in RGB for the study area, distinguishing the ophiolites as violet, the metavolcanics and the metasediments as green, the Hammamat Sediments as bluish and reddish violet, and the younger granites as pink pixels (Fig. 7).

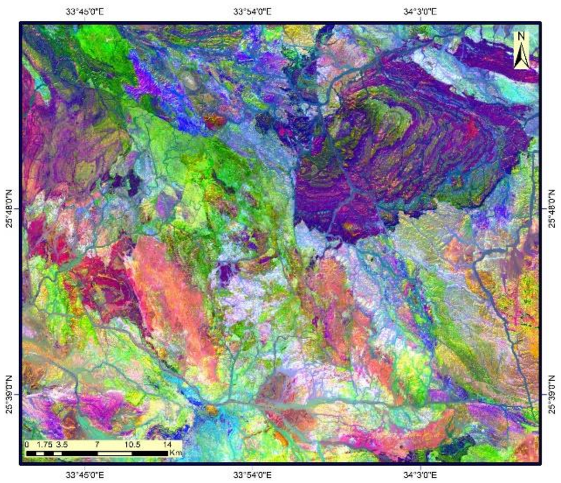


Fig. 7. (C) The RGB band ratio (4/2, 6/5, 6/7) of Wadi Zeidun area effectively distinguishes ophiolites as violet, the metavolcanics and the metasediments as green, the Hammamat Sediments as bluish and reddish violet, and the younger granites as pink-colored pixels.

The results obtained demonstrate the efficacy of LS8OLI data for geological mapping, attributed to the high signal-to-noise ratio present in these multispectral datasets. Field investigations confirm the geological maps created using the BRC and PCA techniques. The findings reveal a strong correlation between the maps produced from the LS8 data and the established geological map. The imagery generated through these processing techniques is more effective at distinguishing the lithological units within the study area. A new geological map of the area under consideration was created by combining the findings from BRC and the PCA analysis with field observations.

Numerous researchers have used remote sensing data to map rock units that may host different types of deposits (e.g. Amer et al., 2012; Amer et al., 2010; Gad and Kusky, 2006a; Gad and Kusky, 2007; Kamel et al., 2022; Mahdy et al., 2024; Othman et al., 2014; Sultan et al., 1986b). For instance, various methods and techniques have been used to identify serpentinized ultramafic rocks, employing tools such as ASTER (Tangestani et al., 2011; Rajendran et al., 2012), Landsat TM (Sultan et al., 1986), and Landsat ETM+ (Gad and Kusky, 2006b) satellite imagery. Previous studies have utilized several image processing methods, including FCC (Pournamdari et al., 2014), PCA (Qaoud, 2014), and band ratios (Sultan et al., 1986a).

Landsat 8 is preferred over ASTER for mapping serpentine due to its better thermal infrared spectral range (12.50 µm for Landsat 8 vs. 11.650 µm for ASTER) and superior coverage, along with being publicly accessible. While ASTER offers finer spatial resolution (15 m for visible and 90 m for TIR) and greater spectral resolution for near-infrared and TIR, Landsat 8 is more cost-effective for mineral exploration compared to imaging spectroscopy. The study employed techniques like FCC, PCA, and ratio images to identify effective detection methods for rock units in the arid Zeidun area. The most effective band ratios were (7/5, 5/4, 6/7) and (4/2, 6/5, 6/7), which enhanced the discrimination and delineation of rock units. The results led to a map that classified the Zeidun area into 13 distinct rock units.

## Conclusions

Remote sensing techniques, such as

BRC analysis and PCA, were employed to analyze LS8OLI data for identifying lithological units of Wadi Zeidun area. These methods proved to be effective, and the outcomes obtained from the PCA images and BRC analysis demonstrated a significant level of consistency. The integration of multispectral optical data from LS8 along with field data has shown to be a valuable approach for lithological mapping, not only in this specific study area but also throughout the entire Egyptian Nubian Shield.

In conclusion, the color composite ratio and the two band ratio techniques (7/5, 5/4, 6/7) and (4/2, 6/5, 6/7) images, whether used with or without supervised classification, yield the most effective results for mapping the rock units and alteration zones in Zeidun area. These band ratio alongside with PCA (432) and FCC (765) successfully mapped the main rock units in the study area including ophiolites, metavolcanics, metasediments, Hammamat Sediments, older and younger granites, and post-Hammamat felsites. Microscopic analysis of the thin sections showed that the alteration minerals present in the study area primarily consist of kaolinite, chlorite, and epidote.

## References

Abd El-Wahed, M., 2007, Late Pan-African tectonic evolution and strain determinations in the Late Neoproterozoic molasse sediments, Eastern Desert, Egypt: evidence for post-Hammamat compression and transpression: Magallat al-"Ulum al-Giyulugiyyat li-l-Gumhuriyyat al-"Arabiyyat al-Muttahidat/United Arab Republic Journal of Geology, v. 51, p. 1.

Abdelsalam, M., and R. Stern, 1999, Mineral exploration with satellite remote sensing imagery: Examples from the Neoproterozoic Arabian-Nubian Shield: Journal of African Earth Sciences, v. 28, p. 1.

Abdelsalam, M. G., C. Robinson, F. El-Baz, and R. J. Stern, 2000a, Applications of orbital imaging radar for geologic studies in arid regions: the Saharan testimony: Photogrammetric Engineering and Remote Sensing, v. 66, p. 717-726.

Abdelsalam, M. G., R. J. Stern, and W. G. Berhane, 2000b, Mapping gossans in arid regions with Landsat TM and SIR-C images: the Beddaho Alteration Zone in northern Eritrea: Journal of African Earth Sciences, v. 30, p. 903-916.

Abrams, M., and A. Kahle, 1984, Recent developments in lithologic mapping using remote sensing data: Remote sensing for geological mapping; Proceedings of the Seminar.

Abrams, M., D. Rothery, and A. Pontual, 1988, Mapping in the Oman ophiolite using enhanced Landsat Thematic Mapper images: Tectonophysics, v. 151, p. 387-401.

Abrams, M. J., D. Brown, L. Lepley, and R. Sadowski, 1983, Remote sensing for porphyry copper deposits in southern Arizona: Economic Geology, v. 78, p. 591-604.

Amer, R., T. Kusky, and A. El, 2012, Remote sensing detection of gold related alteration zones in Um Rus area , Central Eastern Desert of Egypt: Advances in Space Research, v. 49, p. 121-134.

Amer, R., T. Kusky, and A. Ghulam, 2010, Lithological mapping in the Central Eastern Desert of Egypt using ASTER data: Journal of African Earth Sciences, v. 56, p. 75-82.

Ciampalini, A., F. Garfagnoli, B. Antonielli, S. Moretti, and G. Righini, 2013, Remote sensing techniques using Landsat ETM+ applied to the detection of iron ore deposits in Western Africa: Arabian Journal of Geosciences, v. 6, p. 4529-4546.

Clark, R. N., 1999, Spectroscopy of rocks and minerals, and principles of spectroscopy, John Wiley and Sons.

Crosta, A. P., 1989, Enhancement of Landsat Thematic Mapper imagery for residual soil mapping in SW Minas Gerais State Brazil, a prospecting case history in greenstone belt terrain: Proceedings of the 7^< th> ERIM Thematic Conference on Remote Sensing for Exploration Geology, 1989.

Dixon, T. H., 1979, Evolution of continental crust in the Late Precambrian Egyptian Shield, California Univ., San Diego (USA).

El-Shazly, A. K., and K. I. Khalil, 2016, Metamorphic and geochronologic constraints on the tectonic evolution of the Central Eastern Desert of Egypt: Precambrian research, v. 283, p. 144-168.

El-Shazly, A. K., K. I. Khalil, and H. Helba, 2019, Geochemistry of banded iron formations and their host rocks from the Central Eastern Desert of Egypt: a working genetic model and tectonic implications: Precambrian Research, v. 325, p. 192-216.

Evans, D., 1988, Multisensor classification of sedimentary rocks: Remote Sensing of Environment, v. 25, p. 129-144.

Fowler, A.-R., and Z. Hamimi, 2021, Post-amalgamation depositional basins in the Arabian-Nubian Shield: the Hammamat Basins of Egypt: The Geology of the Arabian-Nubian Shield, p. 451-483.

Fowler, A.-R., H. Khamees, and H. Dowidar, 2007, El Sibai gneissic complex, Central Eastern Desert, Egypt: folded nappes and syn-kinematic gneissic granitoid sheets–not a core complex: Journal of African Earth Sciences, v. 49, p. 119-135.

Fowler, A., A. Baghdady, K. Abdelmalik, and A. Gad, 2020, Remote sensing-guided stratigraphic dissection of an Ediacaran terrestrial molasse basin (Kareim basin, Egypt), with implications for sedimentary evolution: Precambrian Research, v. 338, p. 105589.

FREI, M., and S. Jutz, 1990, Use of Thematic Mapper data for the detection of gold bearing formations in the Eastern Desert of Egypt: Thematic conference on remote sensing for exploration geology. Methods, integration, solutions. 7, p. 1157-1172.

Gad, S., and T. Kusky, 2006a, Lithological mapping in the Eastern Desert of Egypt, the Barramiya area, using Landsat thematic mapper (TM): J Afr Earth Sci, v. 44.

Gad, S., and T. Kusky, 2006b, Lithological mapping in the Eastern Desert of Egypt, the Barramiya area, using Landsat thematic mapper (TM): Journal of African Earth Sciences, v. 44, p. 196-202.

Gad, S., and T. Kusky, 2007, GR Letter ASTER spectral ratioing for lithological mapping in the Arabian – Nubian shield , the Neoproterozoic Wadi Kid area , Sinai , Egypt, v. 11, p. 326-335.

Gaffey, S. J., 1986, Spectral reflectance of carbonate minerals in the visible and near infrared (0.35-2.55 microns); calcite, aragonite, and dolomite: American Mineralogist, v. 71, p. 151-162.

Gaffey, S. J., L. A. McFadden, D. Nash, and C. M. Pieters, 1993, Ultraviolet, visible, and near-infrared reflectance spectroscopy: Laboratory spectra of geologic materials: Remote geochemical analysis: Elemental and mineralogical composition, v. 4, p. 43-77.

Ghrefat, H., A. Y. Kahal, K. Abdelrahman, H. J. Alfaifi, and S. Qaysi, 2021, Utilization of multispectral landsat-8 remote sensing data for lithological mapping of southwestern Saudi Arabia: Journal of King Saud University-Science, v. 33, p. 101414.

Hamimi, Z., W. Hagag, H. Fritz, H. Baggazi, and S. Kamh, 2022, The Tectonic Map and Structural Provinces of the Late Neoproterozoic Egyptian Nubian Shield: Implications for Crustal Growth of the Arabian–Nubian Shield (East African Orogen): Frontiers in Earth Science, v. 10, p. 921521.

Hook, S., E. Abbott, C. Grove, A. Kahle, and F. Palluconi, 1999, Use of multispectral thermal infrared data in geological studies: manual of remote sensing (Third Edition, Volume-3), edited by Rencz, AN John Willey and Sons, 699p.

Hunt, G. R., 1977, Spectral signatures of particulate minerals in the visible and near infrared: Geophysics, v. 42, p. 501-513.

FLAASH Module, 2009, Atmospheric correction module: Quac and flaash user's guide: Version, v. 4, p. 44.

Jensen, J., 1996, Introductory Digital Image Processing, PrenticeYHall Series in Geographic Information Science, USa: ISBN 0Y13Y2005840Y5, v. 316.

Kamel, M., A. Tolba, M. M. AbuBakr, and M. M. Omar, 2022, Utilization of Landsat-8 data for lithological mapping of neoproterozoic basement rocks in north Qena-Safaga road, North Eastern Desert, Egypt: Journal of African Earth Sciences, v. 186, p. 104420.

Kassem, O. M. K., M. Abd El-Wahed, A. M. Abudeif, and M. Abdelhameed, 2023, Microstructural and strain studies of neoproterozoic rocks encapsulating hammamat molasse deposits in theWadi El-Qash area, Central Eastern Desert, Egypt: Journal of African Earth Sciences, v. 205.

Kusky, T. M., and T. M. Ramadan, 2002, Structural controls on Neoproterozoic mineralization in the South Eastern Desert, Egypt: an integrated field, Landsat TM, and SIR-C/X SAR approach: Journal of African Earth Sciences, v. 35, p. 107-121.

Lee, D. S., J. C. Storey, M. J. Choate, and R. W. Hayes, 2004, Four years of Landsat-7 on-orbit geometric calibration and performance: IEEE Transactions on Geoscience and Remote Sensing, v. 42, p. 2786-2795.

Loughlin, W., 1991, Principal component analysis for alteration mapping: Photogrammetric Engineering and Remote Sensing, v. 57, p. 1163-1169.

Mahdy, N. M., R. A. El-Arafy, R. A. El-Qassas, M. Metwaly, Y. Abd El-Rahman, H. I. El-Sundolly, and A. Said, 2024, Lithological discrimination of the Fawakhir-Atalla belt in the Central Eastern Desert of Egypt based on Landsat-9 remote sensing data, airborne gamma-ray spectrometry, field and petrographic investigations with implications on the evolution of the Arabian Nubian Shield: Physics and Chemistry of the Earth, Parts A/B/C, v. 134, p. 103578.

Makroum, F., H. Assaf, and G. Saleh, 2001, Tectonic evolution of the basement complex at Wadi Arak area, Central Eastern Desert, Egypt: Egyptian Journal of Geology, v. 45, p. 51-64.

Othman, A. A., R. Gloaguen, R. S. Group, A.-a. Square, and R. S. Group, 2014, remote sensing,

p. 6867-6896.

Pournamdari, M., M. Hashim, and A. B. Pour, 2014, Application of ASTER and Landsat TM Data for Geological Mapping of Esfandagheh Ophiolite Complex , Southern Iran, v. 64, p. 233-246.

Qaoud, N., 2014, Utilization of Space-Borne Imagery for Lithologic Mapping : A Case Study From Um Had Area , Central Eastern Desert , Egypt, v. 6, p. 113-123.

Rajendran, S., B. Pracejus, S. Nasir, A. H. Al-abri, T. M. Kusky, and A. Ghulam, 2012, ASTER detection of chromite bearing mineralized zones in Semail Ophiolite Massifs of the northern Oman Mountains : Exploration strategy: Ore Geology Reviews, v. 44, p. 121-135.

Sabins, F. F., 1999, Remote sensing for mineral exploration: Ore geology reviews, v. 14, p. 157-183.

Sims, P. K., and H. James, 1984, Banded iron-formations of late Proterozoic age in the central Eastern Desert, Egypt; geology and tectonic setting: Economic Geology, v. 79, p. 1777-1784.

Sultan, M., R. Arvidson, and N. C. Sturchio, 1986, Mapping of serpentinites in the Eastern Desert of Egypt by using Landsat thematic mapper data: Geology, v. 14.

Sultan, M., R. E. Arvidson, N. C. Sturchio, and E. A. Guinness, 1987, Lithologic mapping in arid regions with Landsat thematic mapper data: Meatiq dome, Egypt: Geological Society of America Bulletin, v. 99, p. 748-762.

Tangestani, M. H., L. Jaffari, R. K. Vincent, and B. M. Sridhar, 2011, Spectral characterization and ASTER-based lithological mapping of an ophiolite complex: A case study from Neyriz ophiolite, SW Iran: Remote Sensing of Environment, v. 115, p. 2243-2254.

## الملخص العربي

### عنوان البحث: تخريط لصخور النيوبروتيروزوي في الدرع النوبي المصري، بناء على تحيل صور الأقمار الصناعية:حالة دراسية لمنطقة وادي زيدون، النطاق التكتوني المركزي

**محمود ن. التوابتي[١]، هدى رجب سعد[١]، زكريا هميمي[٢]، حسام خميس[٣]، مجدي خليل[١]**

**[١]قسم الجيولوجيا، كلية العلوم، جامعة دمياط، دمياط، مصر**
**[٢]قسم الجيولوجيا، كلية العلوم، جامعة بنها، بنها، مصر**
**[٣] هيئة المواد النووية، القاهرة، مصر**

تقع منطقة الدراسة جنوب طريق قفط-القصير، على طول الحدود الغربية لوسط الصحراء الشرقية. وتغطي المنطقة مجموعة متنوعة من صخور عصر النيوبروتيروزوي، بما في ذلك المتحولة القاتمة اللون، وصخور الجابرو المتحولة، والصخور البركانية المتحولة، والرواسب البركانية المتحولة، والتجمعات القوسية، والجرانيت النيسوسي، والجرانيت القديم والحديث. وتغطي هذه الوحدات بشكل غير متوافق تسلسل بركاني رسوبي بعد الاندماج من رواسب مولاس الحمامات (مجموعة الحمامات). وتوجد بالفعل صخور فلسيت ما بعد الحمامات. ويستكشف العمل الحالي فعالية تقنيات الاستشعار عن بعد، وخاصة استخدام بيانات Landsat-8 إلى جانب بيانات الرحلات الحقلية والخرائط الجيولوجية الموجودة، في رسم خرائط الصخور النيوبروتيروزوي التي تظهر في منطقة شرق وادي زيدون. حيث سهلت بيانات Landsat-8 التعرف على رواسب الحمامات والفلسيت وجرانيتات ما بعد الحمامات من خلال امتداد إزالة الارتباط لمركب الألوان الزائفة 7:6:5 (FCC) في RGB . وقد نجح تحليل المكونات الأساسية (PCA) RGP (PC4,PC3, PC2) في التمييز بين فلسيت ما بعد الحمامات والتجمعات القوسية والجرانيت االاحدث ورواسب الحمامات. بالإضافة إلى ذلك، فإن مجموعات نسب النطاق المحددة (٥/٧، ٤/٥، ٧/٦) و (٢/٤، ٥/٦، ٧/٦) في RGB تجعل من الممكن التمييز بين الأوفيوليتات والبركانيات المتحوله والرواسب المتحولة ورواسب الحمامات والجرانيت الحديث وفلسيت ما بعد الحمامات. وقد تم إثبات النتائج التي تم الحصول عليها من معالجة الصور من خلال الرحلات الحقلية.